



Swansea University
Prifysgol Abertawe



Cronfa - Swansea University Open Access Repository

This is an author produced version of a paper published in:
Geophysical Research Letters

Cronfa URL for this paper:
<http://cronfa.swan.ac.uk/Record/cronfa32971>

Paper:

Hogg, A., Shepherd, A., Cornford, S., Briggs, K., Gourmelen, N., Graham, J., Joughin, I., Mouginot, J., Nagler, T., et al. (2017). Increased ice flow in Western Palmer Land linked to ocean melting. *Geophysical Research Letters*
<http://dx.doi.org/10.1002/2016GL072110>

This item is brought to you by Swansea University. Any person downloading material is agreeing to abide by the terms of the repository licence. Copies of full text items may be used or reproduced in any format or medium, without prior permission for personal research or study, educational or non-commercial purposes only. The copyright for any work remains with the original author unless otherwise specified. The full-text must not be sold in any format or medium without the formal permission of the copyright holder.

Permission for multiple reproductions should be obtained from the original author.

Authors are personally responsible for adhering to copyright and publisher restrictions when uploading content to the repository.

<http://www.swansea.ac.uk/iss/researchsupport/cronfa-support/>

Increased ice flow in Western Palmer Land linked to ocean melting

Anna E. Hogg¹, Andrew Shepherd¹, Stephen L. Cornford^{2,3}, Kate H. Briggs¹, Noel Gourmelen⁴, Jennifer A. Graham⁵, Ian Joughin⁶, Jeremie Mouginot⁷, Thomas Nagler⁸, Antony J. Payne², Eric Rignot^{7,9}, Jan Wuite⁸

¹Centre for Polar Observation and Modelling, School of Earth and Environment, University of Leeds, Leeds, LS2 9JT, UK

²Centre for Polar Observation and Modelling, School of Geographical Sciences, University of Bristol, Bristol, BS8 1SS, UK

³Department of Geography, College of Science, Swansea University, Swansea, SA2 8PP, UK

⁴School of Geosciences, University of Edinburgh, Drummond Street, Edinburgh, EH8 9XP, UK

⁵Met Office, FitzRoy Road, Exeter, Devon, EX13PB, UK

⁶Applied Physics Laboratory, University of Washington, 1013 NE 40th Street, Seattle, Washington, USA

⁷Department of Earth System Science, University of California, Irvine, California, USA

⁸ENVEO IT GmbH, Technikerstrasse 21a, A-6020 Innsbruck, Austria

⁹Jet Propulsion Laboratory, California Institute of Technology, Pasadena, California, USA

Key Points:

- We provide the first observation of changing ice flow in Western Palmer Land.
- Between 1992 and 2015, ice speed and discharge increased by 13 % and 15 km³/yr, respectively.
- The most affected glaciers are deeply grounded and flow into a thinning ice shelf, in an ocean where circumpolar deep water is shoaling.

¹ Corresponding author: Anna E. Hogg, A.E.Hogg@leeds.ac.uk

23 **1. Abstract**

24 A decrease in the mass and volume of Western Palmer Land has raised the prospect that ice
25 speed has increased in this marine-based sector of Antarctica. To assess this possibility, we
26 measure ice velocity over 25 years using satellite imagery and an optimised modelling
27 approach. More than 30 unnamed outlet glaciers drain the 800 km coastline of Western Palmer
28 Land at speeds ranging from 0.5 to 2.5 m/day, interspersed with near-stagnant ice. Between
29 1992 and 2015, most of the outlet glaciers sped up by 0.2 to 0.3 m/day, leading to a 13 %
30 increase in ice flow and a 15 km³/yr increase in ice discharge across the sector as a whole.
31 Speedup is greatest where glaciers are grounded more than 300 m below sea level, consistent
32 with a loss of buttressing caused by ice shelf thinning in a region of shoaling warm circumpolar
33 water.

34 **2. Introduction**

35 Over the past three decades, Antarctica's contribution to global sea level rise has been
36 dominated by ice loss from some of its marine-based sectors [Rignot, 2008; Mouginot et al.,
37 2014; Shepherd et al., 2012]. In particular, glaciers draining the Amundsen Sea Sector of West
38 Antarctica and the Antarctic Peninsula have undergone widespread retreat, acceleration, and
39 thinning [Shepherd et al., 2002; Rignot, 2008; Shuman et al., 2011; Park et al., 2013; McMillan
40 et al., 2014; Mouginot et al., 2014; Rignot et al., 2014; Rott et al., 2014]. These changes have
41 been attributed to the effects of oceanic [Shepherd et al., 2003; Thomas et al., 2008; Jacobs et
42 al., 2011; Cook et al., 2016] and atmospheric [Vaughan and Doake, 1996; Scambos et al., 2000]
43 warming, which has eroded grounded ice and floating ice shelves at the terminus of key marine-
44 based glaciers [Shepherd et al., 2003; 2007; Pritchard et al., 2012], triggering widespread
45 dynamical imbalance upstream [Payne et al., 2004; Joughin et al., 2012; Joughin et al., 2014a].
46 Although observed changes in ice flow at the Antarctic Peninsula have been largely restricted
47 to its northern sectors, there is evidence of recent ice shelf [Shepherd et al., 2010; Pritchard et
48 al., 2012; Paolo et al., 2015] and grounded ice [McMillan et al., 2014; Helm et al., 2014;
49 Wouters et al., 2015] thinning within its southerly glacier catchments, which could impact on
50 future sea level rise.

51 Palmer Land contains the vast majority of the Antarctic Peninsula's ice [Fretwell et al., 2013],
52 and its western flank is drained by glaciers along the English Coast that flow into the George
53 VI and Stange ice shelves (Figure 1) that are predominantly grounded below sea level [Fretwell
54 et al. 2013]. Satellite altimetry has shown that the surface of Western Palmer Land has lowered

55 in recent years [McMillan et al., 2014; Helm et al., 2014], and this has been attributed [Wouters
56 et al., 2015] to an episode of ice dynamic thinning contributing ~ 0.1 mm/yr to global sea level
57 rise. However, because trends in the speed of English Coast glaciers have yet to be documented,
58 this attribution remains speculative. Changes in ice sheet elevation can be caused by changes
59 in surface mass balance or changes in ice flow. Reduced accumulation across a drainage sector
60 leads to surface lowering over short time scales, and this is compensated over time as the ice
61 flow readjusts (slows down) to reduced driving stress. On the other hand, if there is a relative
62 difference in ice speedup along the glacier with greater speedup occurring downstream – which
63 can occur through a variety of internal and external processes – the ice will be stretched and
64 surface lowering will also ensue. Changes in ice flow can, further, be an indicator of dynamic
65 instability, where mass loss leads to a positive feedback mechanism, such as the case of
66 grounding line retreat on a retrograde bedrock slope [Thomas, 1984] in the absence of a
67 compensating mechanism [Gudmundsson et al., 2012]. Because ice sheet surface lowering
68 arising through surface mass or dynamical imbalance have opposing effects on the rate of ice
69 flow, the origin can be established by measuring trends in ice speed. Here, we measure changes
70 in the speed of glaciers draining the English Coast of Western Palmer Land since 1992 to
71 establish what proportion of the reported mass loss [Wouters et al., 2015] is due to temporal
72 variations in ice flow.

73 **3. Data and Methods**

74 We measure changes in Western Palmer Land ice flow using Synthetic Aperture Radar (SAR)
75 and optical satellite images acquired between 1992 and 2016 (Table S1). Ice velocities were
76 computed using a combination of SAR and optical feature tracking [Rosanova et al., 1998;
77 Michel et al., 1999] and SAR interferometry [Goldstein et al., 1988; Joughin et al., 1998]. We
78 tracked the motion of features (including speckle) in sequential SAR images acquired by the
79 Earth Remote Sensing satellites (ERS-1 and -2) in 1992, 1994, and 1996, by the Advanced
80 Land Observation (ALOS) satellite in 2006, 2007, 2008 and 2010, and by the Sentinel-1
81 satellite in 2014, 2015, and 2016, and in sequential optical images acquired by the Landsat-8
82 satellite in 2014. We applied the interferometric technique to repeat pass SAR acquisitions
83 acquired by the ERS-1 and ERS-2 satellites in 1995 and 1996.

84 Feature tracking works by measuring the displacement of features on or near to the ice surface,
85 such as crevasses, rifts and stable amplitude variations, across an observational period. We
86 apply the approach to temporally sequential pairs of Single Look Complex SAR images

87 recorded by ALOS and Sentinel-1, and to optical images recorded by the Landsat-8 Operational
88 Land Imager. SAR image pairs were co-registered using a bilinear polynomial function
89 constrained by precise orbital state vectors. In addition, the co-registration of ERS SAR image
90 pairs was refined with the aid of common features on stable terrain outside areas of fast ice
91 flow, because older mission orbits are less well constrained [Scharroo and Visser, 1998]. Dense
92 networks of local, two-dimensional range and azimuth offsets were then computed from the
93 normalised, cross-correlation of real-valued intensity features present in regularly spaced SAR
94 image patches [Strozzi et al., 2002; Nagler et al., 2015]. Tracked offsets with a signal to noise
95 ratio lower than 4.0 were rejected. Two-dimensional offsets were computed from sequential
96 Landsat-8 images acquired at different times [Mouginot et al., 2014; Fahnestock et al., 2015].
97 To correct the ice motion for sub-pixel geolocation errors in Landsat-8 images, offsets were
98 calibrated by selecting a set of ground control points with zero velocity, and, if not available,
99 slow motion areas [Rignot et al., 2011a].

100 We also use SAR interferometry [Joughin et al., 1998] to derive estimates of ice motion from
101 “tandem” ERS-1 and ERS-2 SAR image pairs acquired one day apart, between March 1995
102 and June 1996. The technique works well on such data, because the relatively short time
103 interval often ensures that phase coherence is preserved over ice sheet surfaces. Temporally
104 sequential SAR image pairs were again co-registered, and their phase signals were interfered
105 on a pixel-by-pixel basis to produce differences that are related to ice motion and topography.
106 The topographic signal was corrected using the satellite SAR imaging geometry and an
107 elevation model [Fretwell et al., 2013], and ice displacement in the SAR range direction was
108 then computed over the image acquisition period from the remaining phase signal. We neglect
109 atmospheric propagation delays, because they are small relative to the signal due to ice flow.
110 Discontinuities arise in the interferometric maps of ice speed where the interferometric phase
111 coherence falls below 0.5.

112 Ice velocity was computed from the feature-tracked and interferometric displacement
113 measurements assuming that the flow is parallel to the surface, and producing a mean speed
114 for the time interval between each image pair. The latter assumption is reasonable, as short-
115 term fluctuations in speed are not apparent in this sector of Antarctica (Figure S4). The spatial
116 resolution of the velocity estimates ranges from 200 to 750 m, and is related to the satellite
117 imaging geometry, the window sizes used in the feature tracking and to the interferometric
118 multi-look processing. Ice velocity estimates derived from each image pair were calibrated,
119 geocoded, and mosaicked together [Mouginot et al., 2012] on a 750 m grid to form regional

120 maps. The estimated accuracy of individual velocity measurements within these maps ranges
121 from 0.01 to 0.06 m/day, on average, depending on the primary data source, the processing
122 technique, and the temporal separation of the satellite image pairs (see Figure S1).

123 **4. Results**

124 Our ice velocity mosaics span 9 distinct epochs, and areas ranging from 810 km² in 1992 to
125 189,109 km² in 2015 (Table S1). Although the extent of measurements from the early 1990's
126 is low, these data provide an important reference for key glaciers to the north of the sector. In
127 all other years, the majority of the ice sheet margin is surveyed, though some mosaics are
128 restricted to the coastal 50-100 km where satellite data were preferentially acquired. Mapping
129 the uppermost reaches of the slow-moving, inland ice is persistently a challenge, due to a
130 paucity of features. We combine velocity measurements derived from satellite images acquired
131 within discrete temporal intervals, and generated using the same processing technique (Table
132 S1), to produce 5 aggregated maps (Figure S1) with broad spatial coverage.

133 The Western Palmer Land coastline is characterised by a 300 km wide central region of ice
134 flowing with indistinct margins between the Horne Nunataks (-71.7° S, -66.7° W) and Eklund
135 Island (-73.2° S, -71.8° W), and by discrete glaciers separated by areas of stagnant flow
136 elsewhere (Figure 1). Ice is transported from the inland Dyer Plateau to the Bellingshausen
137 Sea, mainly via the George VI ice shelf into which most of the regions unnamed glaciers
138 terminate. Of the 30+ glaciers apparent in our velocity data, 10 reach maximum speeds in
139 excess of 1.5 m/day. However, the region of fast flow does not extend far inland, and at
140 distances greater than 100 km from the coast few areas of ice move at speeds greater than 0.25
141 m/day. The region's fastest ice motion occurs at a glacier located opposite the Fauré Inlet on
142 Alexander Island (72.6° S, 70.8° W), where speed exceeds 2.75 m/day.

143 Although the number and distribution of ice flow units in Western Palmer Land has remained
144 constant throughout the 25-year study period, there have been detectable changes in speed in
145 many locations (Figure 2). Nearly all major flow units are surveyed on at least two occasions
146 in our data set (1995 and 2015), with several sampled in all five velocity mosaics (Figure S1).
147 Our time-series shows that the fastest flowing outlet glaciers have sped up by 0.2 to 0.3 m/day
148 since 1992 along their central trunks, with little or no change in the slow flowing inter-glacial
149 regions. Peak speeds occurred at three major ice flow units in 2010 and at one other in 2015
150 (Figure 2), and the average speed of ice across 28,114 km² of the sector increased from 0.31
151 m/day in 1995 to 0.35 m/day in 2015. The largest accelerations occurred within the central

152 portion of Western Palmer Land where the ice flow is generally fastest, and the speedup
153 represents a net loss of ice from the sector because it extends to the coast.

154 Since the satellite observations do not provide complete coverage at each epoch, we
155 compliment them with a set of optimised (calibrated) model ice velocities (Figure S2). The
156 optimisation procedure essentially interpolates the satellite observations in space and time with
157 the aid of an ice flow model [Cornford et al., 2015], assuming spatial and temporal smoothness
158 in the effective basal drag coefficient and the vertically-averaged ice viscosity. This procedure
159 is similar to that of Goldberg et al., [2015], though we seek a time-dependent (rather than time-
160 independent) basal traction coefficient, and depend upon a regularisation term added to the
161 objective function to avoid abrupt temporal variations in the same fashion as abrupt spatial
162 variations. The optimised and observed ice velocity fields agree to within 0.03 m/day, on
163 average, in all epochs (Table S2 and Figure S3), and allow changes in flow to be investigated
164 in areas of data omission (Figure 2).

165 **5. Discussion**

166 We examined changes in ice flow near to the grounding line, where ice discharge occurs, to
167 allow a direct comparison with the estimated mass imbalance of the inland catchment [Wouters
168 et al., 2015]. This region is also where the greatest flow acceleration in response to the reported
169 ice shelf thinning [Shepherd et al., 2010; Pritchard et al., 2012, Paolo et al., 2015] would occur,
170 since longitudinal stresses decay upstream [Schoof, 2007]. Although airborne records of ice
171 thickness and elevation are relatively abundant in Western Palmer Land [Fretwell et al., 2013],
172 we focus on an 800 km coastal flight line (see Figure 1) along which precise measurements
173 were surveyed in 2009 [Allen et al., 2015]. This flight line falls, on average, within 7 km of the
174 grounding line, as determined from satellite radar interferometry [Rignot et al., 2011b]. Our
175 velocity observations sample 86 % and 83 % of the flight line in 1995 and 2015, respectively
176 (Table S1), and the thickest ice (101 and 112 % of the mean thickness, respectively). Ice
177 discharge from the sector was calculated using the observed and modelled ice speed from all 5
178 epochs, and ice thickness across a flux gate located along the airborne flight line (Figure 1).
179 According to the satellite measurements alone, the rate of ice discharge across the commonly-
180 observed, 83 % section of this transect increased by 10 % (from 80 to 88 km³/yr) between 1995
181 and 2015 (Figure 3). For comparison, the model optimisation suggests that ice discharge across
182 the entire gate increased by 11 km³/yr (13 %) over the same period, and that the greatest
183 proportion of ice discharge occurs through the central region (flow unit 3) of Western Palmer

184 Land (Table 1). Furthermore, our model suggests that ice discharge across the gate peaked at
185 $106 \text{ km}^3/\text{yr}$ in 2010, and has dropped since then to $100 \text{ km}^3/\text{yr}$.

186 A number of studies [Helm et al., 2014; McMillan et al., 2014; Wouters et al., 2015] have
187 documented a recent lowering of the grounded ice sheet surface in this sector of Antarctica,
188 with peak rates in the range 2 to 3 m/yr near to the grounding line, leading to an estimated
189 [Wouters et al., 2015] 31 to $43 \text{ km}^3/\text{yr}$ thinning of the inland ice between 2010 and 2014. Our
190 results (Table 1) confirm that part of this thinning is associated with increased ice flow.
191 However, the rate of ice discharge from the sector during the 2010's was only 11 to $15 \text{ km}^3/\text{yr}$
192 greater than during the 1990's, and so increased flow is only responsible for a small fraction
193 (35 %) of the inland thinning. The remainder (65 %) is not associated with dynamical thinning
194 of the inland ice. A possible explanation for the discrepancy lies in the impact of short-term
195 snowfall fluctuations, which are an important and common factor in estimates of ice sheet mass
196 change derived from both satellite altimetry and satellite gravimetry, and which are notoriously
197 difficult to characterise in areas of rugged terrain and high accumulation such as the Antarctic
198 Peninsula [Wouters et al., 2013].

199 To investigate the physical process responsible for the increased ice discharge from Western
200 Palmer Land, we examined the spatial pattern of glacier speedup, which is highly localised
201 (Figure 2). Although lower accumulation may have led to some of the inland deflation, it can
202 be eliminated as a cause of the velocity change because it would reduce the total driving stress
203 over time and, in turn, slow the ice. We must therefore turn to other parts of the force balance
204 for an explanation. The greatest speed up has occurred on glaciers with the fastest initial speed
205 (Figure 1, Figure 2, Figure S5), and these typically flow through deep bedrock troughs (Figure
206 3). This behaviour is in line with theoretical arguments [Schoof, 2007] relating changes in the
207 depth, speed, and instantaneous acceleration of ice flowing across the grounding line in
208 response to changes in ocean forcing or ice stream rheology (either englacial or at the bed)
209 (Figure S5). Satellite altimetry has shown [Shepherd et al., 2010; Paolo et al., 2015] that the
210 George VI ice shelf (into which English Coast glaciers flow) has thinned at rates of between
211 0.8 and 1.0 m/yr since the early 1990's, providing evidence against a (solely) rheological cause
212 for the speedup, which (alone) would lead to ice shelf thickening. This leaves ocean-driven
213 melting, leading to both ice shelf thinning and ice stream speed up, as the remaining possible
214 source of the imbalance.

215 We examined the evidence for the surrounding ocean being the source of the increased ice
216 flow. Warm circumpolar deep water (CDW) is present within the Bellingshausen Sea [Holland
217 et al., 2010] and floods, periodically, through bathymetric depressions onto the continental
218 shelf [Moffat et al., 2009] and into the ocean cavity beneath George VI ice shelf [Potter and
219 Parren, 1985; Talbot, 1988; Jenkins and Jacobs, 2008]. This water is more than 3 °C warmer
220 than the local freezing temperature, and has been recorded at depths below 200 to 300 m in the
221 wider Bellingshausen Sea [Hofmann et al., 2009; Kimura et al., 2015] and at 340 m at the base
222 of George VI ice shelf [Kimura et al., 2015]. Model simulations [e.g. Holland et al., 2010]
223 suggests that it flushes much of the sub-shelf cavity, where it is estimated [Kimura et al., 2015]
224 to generate melting in the range 0.1 to 1.3 m/yr at the base of George VI ice shelf – consistent
225 with the reported ice shelf thinning [Shepherd et al., 2010; Pritchard et al., 2012; Paolo et al.,
226 2015]. Long-term temperature records [Schmidtke et al., 2014] show that the distribution of
227 CDW across the region has shoaled, leading to a 0.1° to 0.3 °C decade⁻¹ warming since 1979 –
228 evidence that the forcing may have increased over time. Despite the regional ice being
229 grounded well below sea level along the majority of the English Coast (Figure 3), significant
230 speedup has only occurred at glaciers that flow along bedrock troughs that are deeper than 300
231 m below present day sea level (Figure 4). However, this pattern corresponds to the depth at
232 which CDW is present (Figure 4c), providing a link between the surrounding ocean and the
233 observed change in ice flow. We hypothesize that ocean driven melting may have triggered
234 modest dynamical thinning of ice in Western Palmer Land – a process that has led to
235 widespread drawdown of inland ice in other sectors of Antarctica [Shepherd et al., 2002;
236 Rignot, 2008; Payne et al., 2004; Joughin et al., 2014a].

237 **6. Conclusions**

238 We provide the first observational evidence that dynamic thinning of ice is occurring at glaciers
239 along the English Coast in Western Palmer Land. Using satellite observations, we show that
240 the rate of ice flow across the sector as a whole has increased by 13 % (from 0.31 to 0.35
241 m/day) since 1995 and, with the aid of an optimised ice sheet model, we show that the rate of
242 ice discharge across a gate near to the grounding line has increased by 13 % (from 88.3 to 99.7
243 km³/yr) over the same period. Though significant, the dynamical imbalance is responsible for
244 only a small proportion (35 %) of the deflation that has occurred inland [Helm et al., 2014;
245 McMillan et al., 2014; Wouters et al., 2015]. The pattern of increased ice flow coincides with
246 the distribution of glaciers that are grounded more than 300 m below sea level, which

247 corresponds to the depth at which warm circumpolar deep water resides within the
248 neighbouring ocean [Hoffman et al., 2009; Kimura et al., 2015]. A large fraction of Western
249 Palmer Land is grounded well below sea level, and so there is a prospect that the ice dynamical
250 imbalance could lead to further draw down of ice from the interior over time – as has occurred
251 in other sectors of Antarctica [Shepherd et al., 2002; Rignot, 2008; Payne et al., 2004; Joughin
252 et al., 2014a]. With enough ice to raise global sea level by over 20 cm [Fretwell et al., 2013],
253 the future evolution of dynamical imbalance in Western Palmer Land should be accounted for
254 in projections of global sea level rise.

255 **7. Acknowledgements**

256 We thank Adrian Jenkins for providing ocean temperature observations. This work was led by
257 the NERC Centre for Polar Observation and Modelling with the support of a grant (No.
258 4000107503/13/I-BG) from the European Space Agency’s Support to Science Element
259 program, and an independent research fellowship (No. 4000112797/15/I-SBo) jointly funded
260 by the European Space Agency, the University of Leeds, and the British Antarctic Survey. The
261 authors gratefully acknowledge the ESA, the National Aeronautics and Space Administration,
262 and the Japan Aerospace Exploration Agency for the use of ERS-1 & -2 (C1P9925), Sentinel-
263 1, Landsat-8, and ALOS PALSAR data, respectively.

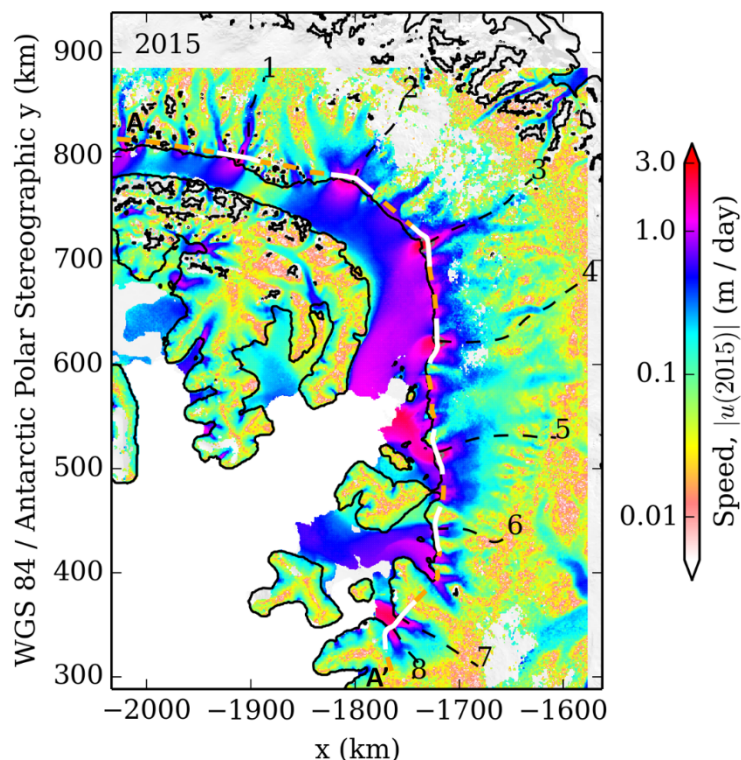


Figure 1. Ice speed (colour) in Western Palmer Land at the Antarctic Peninsula measured in 2015 using repeat pass synthetic aperture radar and optical feature tracking, superimposed on a mosaic of MODIS satellite imagery (grey). Also shown are the locations of the grounding line (black line), the start (A) and end (A') of an airborne flight line where ice thickness was recorded (orange dashed line), flowlines along key outlet glaciers (black, dashed line), and segments of the flowline across which ice discharge is computed (white line).

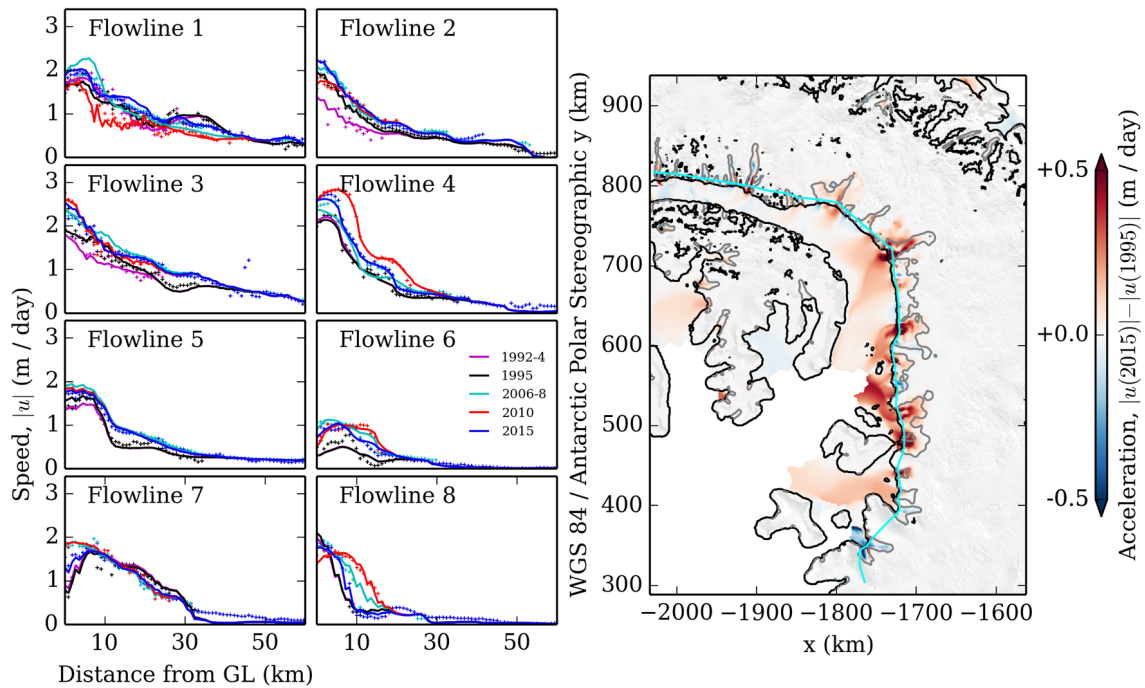


Figure 2. Changes in ice speed in Western Palmer Land measured (symbols) and derived from a model optimisation (lines) along glacier flowlines (see Figure 1) between 1992 and 2015 (left), and a map of ice speedup between 1995 and 2015 (right) derived from a model optimisation of the observed changes (Figure S1, S2 and S5). Also shown are the grounding line (black), the airborne flight line (cyan) and the 300 m/yr ice speed contour (grey).

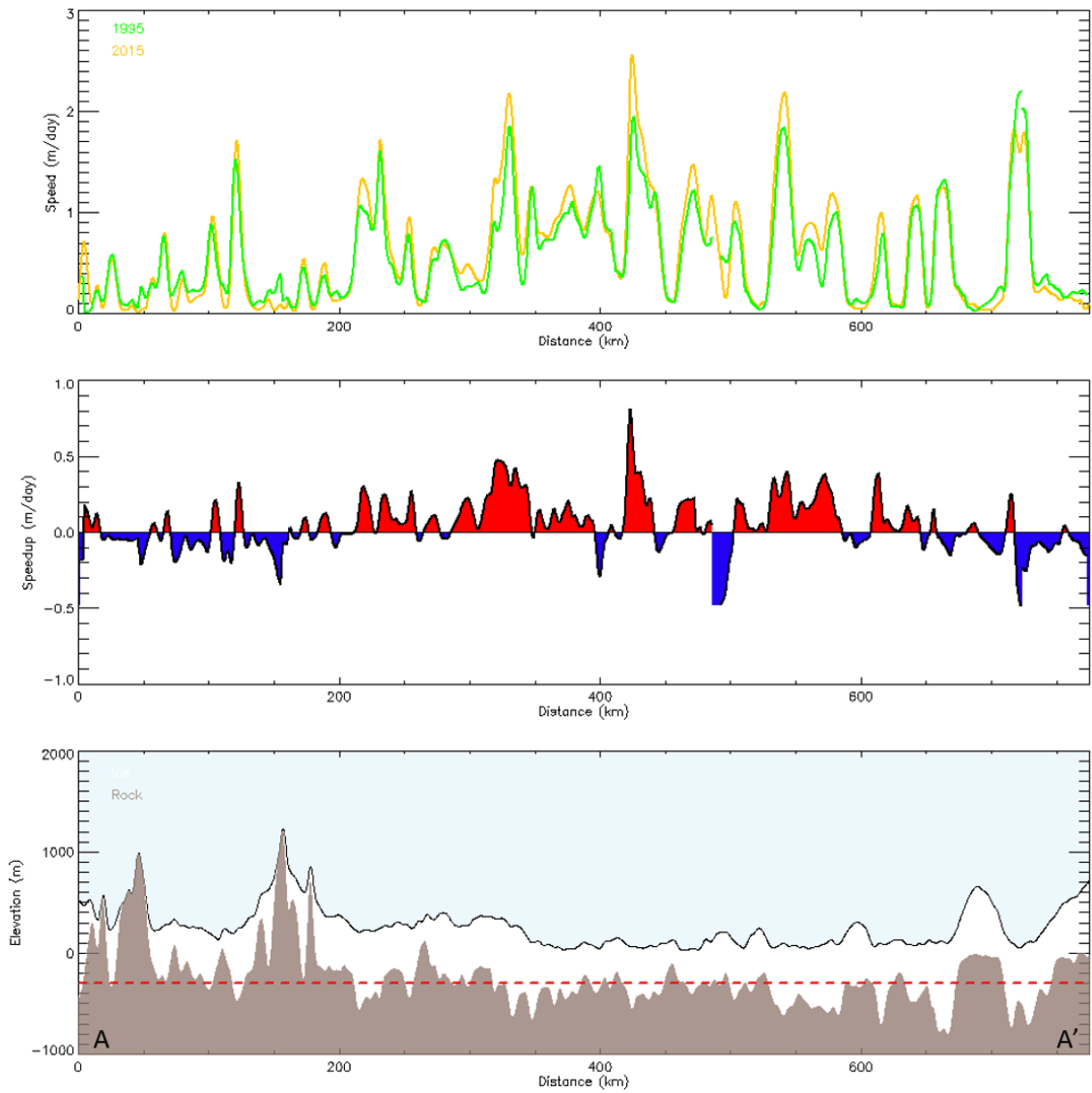


Figure 3. Ice speed (a) in 1995 (green) and 2015 (amber), speedup between 1995 and 2015 (b), and geometry (c) measured along a southerly airborne flight line of the English Coast, Western Palmer Land (see Figure 1). Red dashed line (c) highlights the -300 m bedrock elevation threshold, and the start (A) and end (A') location of the flight line are also annotated.

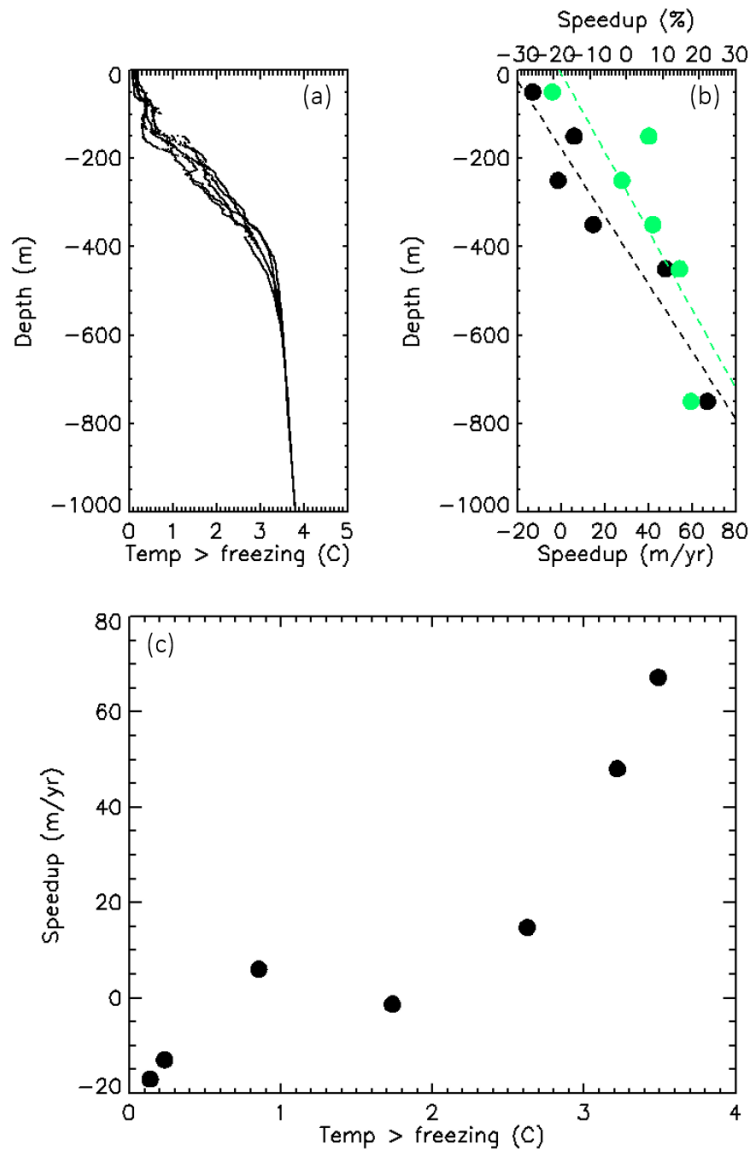


Figure 4. Bellingshausen Sea ocean temperature depth profiles (a). Average variation in absolute (black dots) and relative (green dots) ice speedup along a southerly airborne flight line of the English Coast, Western Palmer Land (see Figure 1) according to the depth at which the ice is grounded below sea level in 100 m elevation bands (b). Average variation in ice speedup along the southerly airborne flight line shown against ocean temperature at the corresponding depth below present day sea level (c).

268

Year	Unit 1 km ³ /yr	Unit 2 km ³ /yr	Unit 3 km ³ /yr	Unit 4 km ³ /yr	Unit 5 km ³ /yr	Unit 6 km ³ /yr	Unit 7 km ³ /yr	Unit 8 km ³ /yr	Rest km ³ /yr	All km ³ /yr
1992-6	4.0	6.2	9.4	8.6	6.1	1.5	9.1	9.6	29.6	84.5
1995-6	3.7	8.5	10.3	8.5	6.9	1.5	9.4	9.9	29.6	88.3
2006-8	4.6	9.9	12.9	10.0	8.4	2.7	8.9	9.3	35.3	102.0
2010	4.4	10.0	14.9	11.5	8.7	2.3	8.2	8.5	37.7	106.4
2014-16	4.0	9.4	13.4	10.6	8.3	2.3	8.2	8.5	35.1	99.7

Table 1. Ice discharge across 40 km wide segments of a southerly airborne flight line of the English Coast, Western Palmer Land (see Figure 1) computed from model optimised ice

velocity data. Locations and epochs where 25 % or less of the segments were constrained with observations are italicised.

269 **9. References**

- 270 Allen, C., C. Leuschen, P. Gogineni, F. Rodriguez-Morales, J. Paden (2010), updated 2015,
271 IceBridge MCoRDS L2 Ice Thickness, [IRMCR2_20091103_02], Boulder, Colorado USA,
272 *NASA National Snow and Ice Data Center Distributed Active Archive Center*,
273 <http://dx.doi.org/10.5067/GDQ0CUCVTE2Q>.
- 274 Cook, A. J., P. R. Holland, M. P. Meredith, T. Murray, A. Luckman, D. G. Vaughan, (2016)
275 Ocean forcing of glacier retreat in the western Antarctic Peninsula, *Science*, 353, (6296), 283-
276 286, doi: 10.1126/science.aae0017.
- 277 Cornford, S. L., D. F. Martin, A. J. Payne, E. G. Ng, A. Le Brocq, R. M. Gladstone, T. L.
278 Edwards, S. R. Shannon, C. Agosta, M. R. van den Broeke, H. Hellmer, G. Krinner, S. R. M.
279 Ligtenberg, R. Timmermann, D. G. Vaughan, (2015) Century-scale simulations of the response
280 of the West Antarctic Ice Sheet to a warming climate, *The Cryosphere*, 9, 1579-1600,
281 doi:10.5194/tc-9-1579-2015.
- 282 Fretwell, P., H. D. Pritchard, D. G. Vaughan, J. L. Bamber, N. E. Barrand, R. Bell, C.
283 Bianchi, R. G. Bingham, D. D. Blankenship, G. Casassa, G. Catania, D. Callens, H. Conway,
284 A. J. Cook, H. F. J. Corr, D. Damaske, V. Damm, F. Ferraccioli, R. Forsberg, S. Fujita, Y.
285 Gim, P. Gogineni, J. A. Grigg, R. C. A. Hindmarsh, P. Holmlund, J. W. Holt, R. W. Jacobel,
286 A. Jenkins, W. Jokat, T. Jordan, E. C. King, J. Kohler, W. Krabill, M. Riger-Kusk, K. A.
287 Langley, G. Leitchenkov, C. Leuschen, B. P. Luyendyk, K. Matsuoka, J. Mouginot, F. O.
288 Nitsche, Y. Nogi, O. A. Nost, S. V. Popov, E. Rignot, D. M. Rippin, A. Rivera, J. Roberts, N.
289 Ross, M. J. Siegert, A. M. Smith, D. Steinhage, M. Studinger, B. Sun, B. K. Tinto, B. C. Welch,
290 D. Wilson, D. A. Young, C. Xiangbin, A. Zirizzotti, (2013) Bedmap2: Improved ice bed,
291 surface and thickness datasets for Antarctica, *The Cryosphere*, 7, 375–393, doi:10.5194/tc-7-
292 375-2013.
- 293 Fahnestock, M., T. Scambos, T. Moon, A. Gardner, T. Haran, M. Klinger, (2015) Rapid
294 large-area mapping of ice flow using Landsat 8, *Remote Sensing of Environment*, 185, 84 –
295 94, doi:10.1016/j.rse.2015.11.023.
- 296 Goldberg, D. N., P. Heimbach, I. Joughin, B. Smith, (2015) Committed retreat of Smith, Pope,
297 and Kohler Glaciers over the next 30 years inferred by transient model calibration, *The*
298 *Cryosphere*, 9, 2429–2446, doi:10.5194/tc-9-2429-2015.
- 299 Goldstein, R. M., H. A. Zebker, C. L. Werner, (1988) Satellite radar interferometry: Two-
300 dimensional phase unwrapping, *Radio Science*, 23, 4, 713-720,
301 doi:10.1029/RS023i004p00713.

302 Gudmundsson, G. H., J. Krug, G. Durand, L. Favier, O. Gagliardini, (2012) The stability of
303 grounding lines on retrograde slopes, *The Cryosphere*, 6, 1497-1505, doi:10.5194/tc-6-1497-
304 2012.

305 Helm, V., A. Humbart, H. Miller, (2014) Elevation and elevation change of Greenland and
306 Antarctica derived from CryoSat-2, *The Cryosphere*, 8, 1539 - 1559, doi:10.5194/tc-8-1539-
307 2014.

308 Hofmann, E. E., D. P. Costa, K. Daly, M. S. Dinniman, J. M. Klinck, M. Marrari, L. Padman,
309 A. Piñones, (2009) Results from the US Southern Ocean GLOBEC synthesis studies, *GLOBEC*
310 *Int. Newsl.*, 15, 43–48. Holland, P.R., A. Jenkins, D. M. Holland, (2010) Ice and ocean
311 processes in the Bellingshausen Sea, Antarctica, *Journal of Geophysical Research: Oceans*,
312 115(C5), C05020, doi: 10.1029/2008JC005219.

313 Jacobs, S. S., A. Jenkins, C. F. Giulivi, P. Dutrieux, (2011) Stronger ocean circulation and
314 increased melting under Pine Island Glacier ice shelf, *Nat. Geosci.*, 4, 519–523, doi:
315 10.1038/ngeo1188.

316 Jenkins, A., and S. Jacobs, (2008) Circulation and melting beneath George VI Ice Shelf,
317 Antarctica, *Journal of Geophysical Research*, 113. 10.1029/2007JC004449.

318 Joughin, I. R., R. Kwok, M. A. Fahnestock, (1998) Interferometric estimation of three-
319 dimensional ice-flow using ascending and descending passes, *IEEE Trans. Geosci. Remote*
320 *Sens.*, 36, 25–37, doi:10.1109/36.655315.

321 Joughin, I., S. Tulaczyk, J. L. Bamber, D. Blankenship, J. W. Holt, T. Scambos, D. G. Vaughan,
322 (2009) Basal conditions for Pine Island and Thwaites Glaciers, West Antarctica, determined
323 using satellite and airborne data, *J. Glaciol.*, 55, 245–257, doi:10.3189/002214309788608705.

324 Joughin, I., R. B. Alley, D. M. Holland, (2012) Ice-Sheet Response to Oceanic Forcing,
325 *Science*, 338, 1172 – 1176, doi:10.1126/science.1226481.

326 Joughin, I., B. E. Smith, B. Medley, (2014a) Marine ice sheet collapse potentially underway
327 for the Thwaites Glacier basin, West Antarctica, *Science*, 344, 735-738,
328 doi:10.1126/science.1249055.

329 Joughin, I., B. Smith, D. E. Shean, D. Floricioiu (2014b) Brief communication: Further summer
330 speedup of Jakobshavn Isbrae, *The Cryosphere*, 8, 209 – 214, doi:10.5194/tc-8-209-2014.

331 Kimura, S., K. W. Nicholls, E. Venables (2015) Estimation of Ice Shelf Melt Rate in the
332 Presence of a Thermohaline Staircase, *Journal of Oceanography*, 45, 133–148 ,
333 doi:10.1175/JPO-D-13-0219.1.

334 MacAyeal, D. R. (1993) A tutorial on the use of control methods in ice- sheet modeling, *J.*
335 *Glaciol.*, 39, 91–98.

336 McMillan, M., A. Shepherd, A. Sundal, K. Briggs, A. Muir, A. Ridout, A. Hogg, D. Wingham,
337 (2014) Increased ice losses from Antarctica detected by CryoSat-2, *Geophysical Research*
338 *Letters*, 41, 3899-3905, 10.1002/2014GL060111.

339 Michel, R., and E. Rignot, (1999) Flow of Glaciar Moreno, Argentina, from repeat-pass Shuttle
340 Imaging Radar images: Comparison of the phase correlation method with radar interferometry,
341 *J. Glaciol.*, 45, 93–100.

342 Moffat, C., B. Owens, R. C. Beardsley, (2009) On the characteristics of Circumpolar Deep
343 Water intrusions to the west Antarctic Peninsula continental shelf, *J. Geophys. Res.*, 114,
344 C05017, doi:10.1029/2008JC004955.

345 Moon, T., I. Joughin, B. Smith, M. R. van den Broeke, W. J. van de Berg, B. Noël, M. Usher
346 (2014) Distinct patterns of seasonal Greenland glacier velocity, *Geophysical Research Letters*,
347 41, 7209 – 7216, doi:10.1002/2014GL061836.

348 Morlighem, M., E. Rignot, H. Seroussi, E. Larour, H. Den Bhia, D. Aubry, (2010) Spatial
349 patterns of basal drag inferred using control methods from a full-Stokes and simpler models
350 for Pine Island Glacier, West Antarctica, *Geophys. Res. Lett.*, 37, L14502,
351 doi:10.1029/2010GL043853.

352 Mouginot, J., B. Scheuchl, E. Rignot, (2012) Mapping of ice motion in Antarctica using
353 synthetic-aperture radar data, *Journal of Remote Sensing*, 4(9), 2753-2767,
354 doi:10.3390/rs4092753.

355 Mouginot, J., E. Rignot, B. Scheuchl, (2014) Sustained increase in ice discharge from the
356 Amundsen Sea Embayment, West Antarctica, from 1973 to 2013, *Geophys. Res. Lett.*, 41,
357 doi:10.1002/2013GL059069.

358 Nagler, T., H. Rott, M. Hetzenecker, J. Wuite, (2015) The Sentinel-1 Mission: New
359 Opportunities for Ice Sheet Observations, *Remote Sens.* 7, 9371 – 9389,
360 doi:10.3390/rs70709371.

361 Paolo, F.S., H. A. Fricker, L. Padman, (2015) Volume loss from Antarctic ice shelves is
362 accelerating, *Science*, 348, (6232), 327–331, doi:10.1126/science.aaa0940.

363 Park, J. W., N. Gourmelen, A. Shepherd, S. W. Kim, D. G. Vaughan, D. J. Wingham, (2013)
364 Sustained retreat of the Pine Island Glacier, *Geophys. Res. Lett.*, 40, 2137–2142,
365 doi:10.1002/grl.50379.

366 Payne, A. J., A. Vieli, A. P. Shepherd, D. J. Wingham, E. Rignot, (2004) Recent dramatic
367 thinning of largest West Antarctic ice stream triggered by oceans, *Geophys. Res. Lett.*, 31,
368 L23401, doi:10.1029/2004GL021284.

369 Potter, J. R., and J. G. Paren, (1985) Interaction between ice shelf and ocean in George VI
370 Sound, Antarctica, *Antarct. Res. Ser.*, 43, 35- 58, doi:10.1029/AR043p0035.

371 Pritchard, H. D., S. R. M. Ligtenberg, H. A. Fricker, D. G. Vaughan, M. R. van den Broeke,
372 and L. Padman, (2012) Antarctic ice-sheet loss driven by basal melting of ice shelves, *Nature*,
373 484, 502–505, doi:10.1038/nature10968.

374 Rignot, E., J. Bamber, M. van den Broeke, C. Davis, Y. Li, W. van de Berg, E. van Meijgaard,
375 (2008) Recent Antarctic ice mass loss from radar interferometry and regional climate
376 modelling, *Nat. Geosci.*, 1(2), 106–110, doi:10.1038/ngeo102.

377 Rignot, E., J. Mouginot, B. Scheuchl, (2011a), Ice flow of the Antarctic Ice Sheet, *Science*,
378 333, 6048, 1427 – 1430, doi:10.1126/science.1208336.

379 Rignot, E., J. Mouginot, B. Scheuchl, (2011b), Antarctic grounding line mapping from
380 differential satellite radar interferometry, *Geophys. Res. Lett.*, 38, L10504,
381 doi:10.1029/2011GL047109.

382 Rignot, E., J. Mouginot, M. Morlighem, H. Seroussl, B. Scheuchl, (2014) Widespread, rapid
383 grounding line retreat of Pine Island, Thwaites, Smith and Kohler glaciers, West Antarctica,
384 *Geophysical Research Letters*, 41, 3502 – 3509, doi:10.1002/2014GL060140.

385 Rosanova, C. E., B. K. Lucchitta, J. G. Ferrigno, (1998) Velocities of Thwaites Glacier and
386 smaller glaciers along the Marie Byrd Land coast, West Antarctica, *Ann. Glaciol.*, 27, 47–53,
387 doi:10.3189/172756494794587573.

388 Rott, H., D. Floricioiu, J. Wuite, S. Scheiblauer, T. Nagler, M. Kern, (2014) Mass changes of
389 outlet glaciers along the Nordenskjöld Coast, northern Antarctic Peninsula, based on TanDEM-
390 X satellite measurements, *Geophys. Res. Lett.*, 41, 8123–8129, doi:10.1002/2014GL061613.

391 Scambos, T. A., C. Hulbe, M. Fahenstock, J. Bohlander, (2000) The link between climate
392 warming and break-up of ice shelves in the Antarctic Peninsula, *Journal of Glaciology*, 46,
393 154, 516 – 530, doi:10.3189/172756500781833043.

394 Schoof, C. (2007) Ice sheet grounding line dynamics: steady states, stability and hysteresis,
395 *Journal of Geophysical Research*, 112, F03S28, doi:10.1029/2006JF000664.

396 Scharroo, R. and Visser, P. (1998) Precise orbit determination and gravity field improvement
397 for the ERS satellites, *Journal of Geophysical Research*, 103, C4, 8113-8127,
398 doi:10.1029/97JC03179.

399 Schmidtko, S., K. J. Haywood, A. F. Thompson, A. Aoki, (2014) Multidecadal Warming of
400 Antarctic Waters, *Science*, 346, 2614, 1227 – 1231, doi:10.1126/science.1256117.

401 Shepherd, A., D. Wingham, J. A. D. Mansley, (2002) Inland thinning of the Amundsen Sea
402 sector, West Antarctica, *Geophys. Res. Lett.*, 29, (10), 1364, 10.1029/2001GL014183.

403 Shepherd, A., D. Wingham T. Payne, P. Skvarca, (2003) Larsen ice shelf has progressively
404 thinned, *Science*, 302, 5646, 856 – 859, doi:10.1126/science.1089768.

405 Shepherd, A., D. Wingham, (2007) Recent sea-level contributions of the Antarctic and
406 Greenland Ice Sheets, *Science*, 315, 1529 – 1532, doi:10.1126/science.1136776.

407 Shepherd, A., D. Wingham, D. Wallis, K. Giles, S. Laxon, A. V. Sundal, (2010) Recent loss
408 of floating ice and the consequent sea level contribution, *Geophysical Research Letters*, 37,
409 L13503, doi: 10.1029/2010GL042496.

410 Shepherd, A., E. R. Ivins, G. A. V. R. Barletta, M. J. Bentley, S. Bettadpur, K. H. Briggs, D.
411 H. Bromwich, R. Forsberg, N. Galin, M. Horwath, S. Jacobs, I. Joughin, M. A. King, J. T. M.
412 Lenaerts, J. Li, S. R. M. Ligtenberg, A. Luckman, S. B. Luthcke, M. McMillan, R. Meister, G.
413 Milne, J. Mouginot, A. Muir, J. P. Nicolas, J. Paden, A. J. Payne, H. Pritchard, E. Rignot, H.
414 Rott, L. S. Sørensen, T. A. Scambos, B. Scheuchl, E. J. O. Schrama, B. Smith, A. V. Sundal,
415 J. H. van Angelen, W. J. van de Berg, M. R. van den Broeke, D. G. Vaughan, I. Velicogna, J.
416 Wahr, P. L. Whitehouse, D. J. Wingham, D. Yi, D. Young, H. J. Zwally, (2012) A reconciled
417 estimate of ice-sheet mass balance, *Science*, 338, 1183- 1189, doi:10.1126/science.1228102.

418 Shuman, C. A., E. Berthier, T. A. Scambos, (2011) 2001-2009 elevation and mass losses in the
419 Larsen A and B embayments, Antarctic Peninsula, *Journal of Glaciology*, 57(204), 737-754,
420 doi:10.3189/002214311797409811.

421 Strozzi, T., A. Luckman, T. Murray, U. Wegmuller, C. L. Werner, (2002) Glacier motion
422 estimation using SAR offset-tracking procedures, *IEEE Transactions on Geoscience and*
423 *Remote Sensing*, 40, 2384–2391, doi:10.1109/TGRS.2002.805079.

424 Talbot, M.H. (1988) Oceanic environment of George VI Ice Shelf, Antarctic Peninsula, *Annals*
425 *of Glaciology*, 11, 161-164.

426 Thomas, E. R., G. J. Marshall, J. R. McConnell, (2008) A doubling in snow accumulation in
427 the western Antarctic Peninsula since 1850, *Geophys. Res. Lett.* 35, L01706,
428 doi:10.1029/2007GL032529.

429 Thomas, R. H. (1984) Ice Sheet Margins and Ice Shelves, in *Climate Processes and Climate*
430 *Sensitivity* (eds. J. E. Hansen and T. Takahashi), American Geophysical Union, Washington,
431 D. C. doi:10.1029/GM029p0265.

432 Vaughan, D. G., and C. S. M. Doake, (1996) Recent atmospheric warming and retreat of ice
433 shelves on the Antarctic Peninsula, *Nature*, 379, 328–331, doi:10.1038/379328a0.

434 Wouters, B., J. L. Bamber, M. R. van den Broeke, J. T. M. Lenaerts, I. Sasgen, (2013) Limits
435 in detecting acceleration of ice sheet mass loss due to climate variability, *Nature Geoscience*,
436 6, 613 – 616, doi:10.1038/ngeo1874.

437 Wouters, B., A. Martín-Español, V. Helm, T. Flament, J. M. van Wessem, S. R. M. Ligtenberg,
438 M. R. van den Broeke, J. L. Bamber, (2015) Dynamic thinning of glaciers on the Southern
439 Antarctic Peninsula, *Science*, 348, 899-903, doi:10.1126/science.aaa5727.